WP17ER-PR(18) 20695

L Sanchis-Sanchez et al.

Fast-ion edge resonant transport layer induced by externally applied 3D perturbative fields in the ASDEX Upgrade tokamak

Preprint of Paper to be submitted for publication in
Physical Review Letters

This work has been carried out within the framework of the EUROfusion Consortium and has received funding from the Euratom research and training programme 2014-2018 under grant agreement No 633053. The views and opinions expressed herein do not necessarily reflect those of the European Commission.

Fast-Ion Edge Resonant Transport Layer Induced by Externally Applied 3D Perturbative Fields in the ASDEX Upgrade Tokamak

L. Sanchis[1,2], M. Garcia-Munoz[1,2], A. Snicker[3], J. Galdon-Quiroga[1,2], D. A. Ryan[4], M. Nocente[5], J. F. Rivero-Rodriguez[1,2], L. Chen[6], W. Suttrop[7], E. Viezzer[1,2], M. A. Van Zeeland[8], M. Willensdorfer[7], F. Zonca[9], D. Zarzoso[10], the ASDEX Upgrade Team and the EUROfusion MST1 Team

[1] *Dept. of Atomic, Molecular and Nuclear Physics, University of Seville, Avda. Reina Mercedes, 41012 Seville, Spain*

[2] *Centro Nacional de Aceleradores CNA (Universidad de Sevilla, Junta de Andalucia, CSIC), Avda. Thomas A. Edison 7, 41092 Seville, Spain*

[3] *Dept. of Applied Physics, Aalto University, FI- 00076, Aalto, Finland*

[4] *CCFE, Culham Science Centre, OX14 3DB, Abingdon, UK*

[5] *Universita degli Studi di Milano-Bicocca, Piazza della Scienza 3, 20126, Milano, Italy*

[6] *IFTS, Zhejiang University, 310027, 310027, Hangzhou, China*

[7] *Max Planck Institute for Plasma Physics, Boltzmannstr. 2, 85748 Garching, Germany*

[8] *General Atomics, CA 92186-5608, San Diego, USA*

[9] *ENEA C.R. Frascati, CP 65-00044, Frascati, Italy and*

[10] *Aix-Marseille Université, CNRS, PIIM, UMR 7345, Mareseille, France*

Recent experiments in the ASDEX Upgrade tokamak have revealed the existence of an edge resonant transport layer responsible for the observed fast-ion losses in the presence of externally applied 3D fields. The amplitude of the observed fast-ion losses depends strongly on the energetic particle phase space and poloidal mode spectra of the external perturbation. Numerical and analytical results show that the combination of multiple non-linear resonances with the applied perturbative fields create a transport layer that depends on the perturbation spectra, magnetic equilibrium and particle orbit topology and collisionality. The ability to create a resonant transport layer at the edge of a tokamak plasma opens new avenues for the control of the energetic particle population and associated magnetohydrodynamic fluctuations in future burning plasmas.

Toroidal symmetry is the basis of magnetically confined fusion devices. Nested flux surfaces and particles constants of motion ensure plasma confinement in tokamaks and stellarators. Symmetry breaking 3D fields can, however, modify the overall plasma confinement and stability [1]. In stellarators, the magnetic field is created without the induced plasma current and, thus, external 3D fields are intrinsically present. In tokamaks, 3D perturbative fields may be mandatory to preserve the device integrity against intolerable plasma fluctuations such as locked modes [2], Edge Localised Modes (ELMs) [3–5], Resistive Wall Modes (RWMs)[6] and Alfvén Eigenmodes (AEs) [7].

The impact that externally applied 3D fields have on the overall plasma stability and confinement is, however, complicated by several simultaneous non-linear effects that compete at different spatio-temporal scales. These effects include the magnetic equilibrium, main plasma parameters and perturbation spectrum. 3D fields can excite kink [8], which induces internal currents [9] and can amplify the external perturbation modifying significantly the plasma stability [10], magnetic topology (or Resonant Field Penetration) [11] and thermal particle exhaust [12]. Energetic particles are especially sensitive to this complex 3D magnetic background due to their relatively long mean free path and slowing down times [13, 14].

The theory of particle transport in 3D toroidal devices has been extensively studied in the banana-drift regime [15], where small 3D perturbations fields can have a strong impact on overall plasma parameters through nonambipolar thermal particle transport [16]. Bounce-harmonic resonances have been found numerically [17] to greatly enhance the thermal particle transport in the relatively high collisionality $1/\nu$ [18] and low collisionality $\nu_-\sqrt{\nu}$ [19] regimes. Low collisionality energetic particles have been predicted to be subject to a large resonant transport in the presence of symmetry breaking 3D fields [20].

In this letter we present the first evidence of a fast-ion Edge Resonant Transport Layer (ERTL) in a tokamak with externally applied 3D perturbative fields. Full-orbit simulations indicate that the increased fast-ion transport occurs in a thin layer around the plasma boundary where analytical theory predicts an interaction of multiple linear and non-linear resonances between the fast-ion orbits and the applied 3D perturbative fields. Good agreement is found between the experimental observation, the numerical results and the analytical theory. The ERTL properties depend strongly on the fast-ion orbit topology and relative phase with respect to the perturbation, on the perturbation spectra, magnetic equilibrium helicity and collisionality. This ERTL appears to be an essential element in optimizing fast-ion confinement in tokamaks with externally applied magnetic perturbations such as ITER.

Experiment - The experiment discussed here was carried out in the ASDEX Upgrade (AUG) tokamak in an

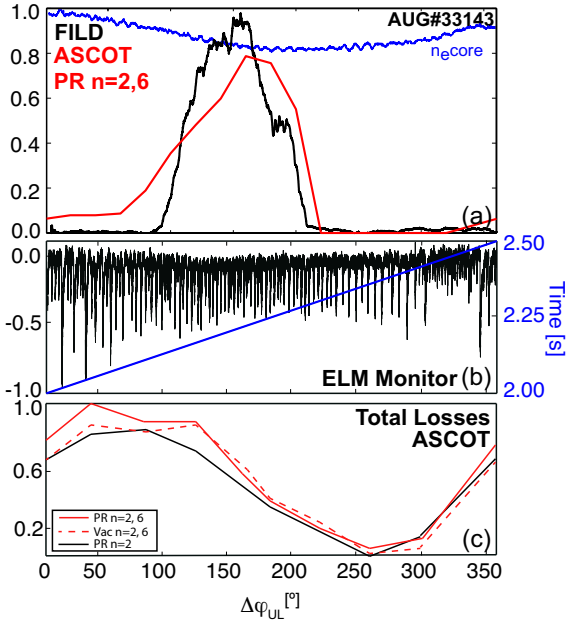

FIG. 1. AUG#33143. (a) Normalized values of measured (black) and simulated with ASCOT (red) FILD signals as a function of the applied $\Delta\varphi_{UL}$, the line integrated core density is overplotted in blue. (b) Poloidal thermo-currents from the outer divertor target plates showing ELM mitigation as a function of the applied current phase $\Delta\varphi_{UL}$ and time window corresponding to the analysed $\Delta\varphi_{UL}$ (blue). (c) Total fast-ions losses as a function of $\Delta\varphi_{UL}$ including n=2 plasma response (black), n=2 and n= 6 plasma response (red) and n=2 and n=6 vacuum fields (red dashed line).

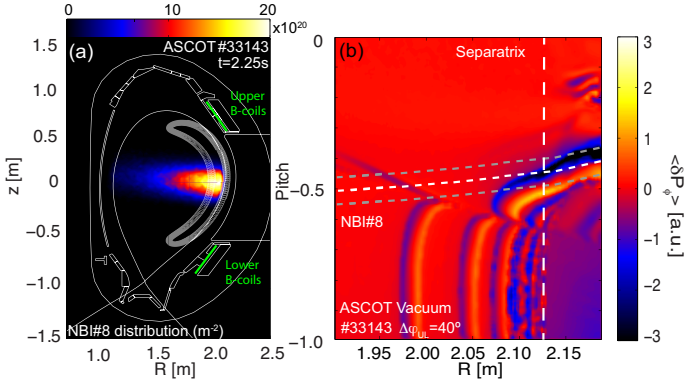

FIG. 2. AUG#33143. (a) Poloidal cross-section of the AUG vacuum vessel showing the NBI birth distribution and a representative particle orbit. (b) $\langle\delta P_\phi\rangle$ as function of particle pitch-angle and plasma major radius for a $\Delta\varphi_{UL} = 40°$ and particle energy E=60keV including the fast-ion distribution maximum (white) and FWHM (grey)

ELMy H-mode plasma with a toroidal magnetic field at the magnetic axis, $B_t = 1.8\,\mathrm{T}$, a plasma current, $I_P = 0.8\,\mathrm{MA}$, a normalized ratio of plasma pressure to magnetic pressure, β_N=2.4 and a collisionality $\nu_e^* \approx 0.2$. 2 MW of Electron Cyclotron Resonance Heating (ECRH) power was used to heat the plasma centre up to several keV. The fast-ions studied here were generated by means of 5 MW of Neutral Beam Injection (NBI). A n=2 Resonant Magnetic Perturbation (RMP) was applied by two sets of eight ELM control coils, one above the midplane and one below [21]. The current flowing through the lower set of coils was kept at a constant toroidal phase (ϕ_L) while the upper set of coils (ϕ_U) was rotating at 2 Hz, introducing a differential phase shift ($\Delta\varphi_{UL} = \phi_U - \phi_L$) that covered a continuous scan in the poloidal mode spectra. Density pump out and partial ELM mitigation were observed when the coils were turned on (Figs. 1(a) and 1(b)), both showing a clear modulation with the poloidal mode spectra of the applied perturbation. The effect of this modulation was especially clear in the fast-ion loss detector (FILD) [22] measurements (Fig. 1(a)), where fast-ion losses were only detected for a certain poloidal spectrum of the applied perturbation within a narrow window between $\Delta\varphi_{UL} = 120°$ and $\Delta\varphi_{UL} = 230°$ with an energy $E \approx 50$keV and a pitch $\Lambda = v_\parallel/v_{tot} = -0.5$.

Modelling - The physics mechanism underlying the observed fast-ion transport in the presence of externally applied 3D fields with different poloidal mode spectra has been studied numerically using the Monte Carlo orbit-following code ASCOT [23]. Realistic 3D wall geometry, fast-ion distribution and perturbed fields, including the plasma response as calculated with the MARS-F code [24] have been considered. Figure 2(a) shows a poloidal projection of the NBI fast-ion birth distribution with a typical particle trajectory overplotted in white. The pitch-angle distribution of the injected particles as a function of plasma major radius is shown in Fig. 2(b) for the main injection energy component as white dotted line with full width half maximum as grey dotted line. The plasma response to the main harmonics, n=2 and n=6, of the externally applied perturbation has been calculated for each coil configuration, i.e. perturbation poloidal mode spectra. A reasonable agreement is obtained between the simulated and experimentally measured fast-ion losses at the FILD detector as a function of the perturbation poloidal spectrum as Fig. 1(a) shows. Both FILD measurements and ASCOT results show significant losses for a $\Delta\varphi_{UL}$ between 100° and 200° with the maximum peaked at $\Delta\varphi_{UL} \approx 180°$. The total fast-ion losses registered at the first wall peak, however, for a $\Delta\varphi_{UL}$ between 50° and 100° with the minimum at $\Delta\varphi_{UL} \approx 250°$ as Fig. 1(c) shows. Most fast-ion losses are caused by the main n=2 perturbation while n=6 side harmonics enhance the simulated losses up to 20% for certain poloidal mode spectra highlighting the importance of the perturbation poloidal structure for the energetic particle confinement. Significant differences are observed between

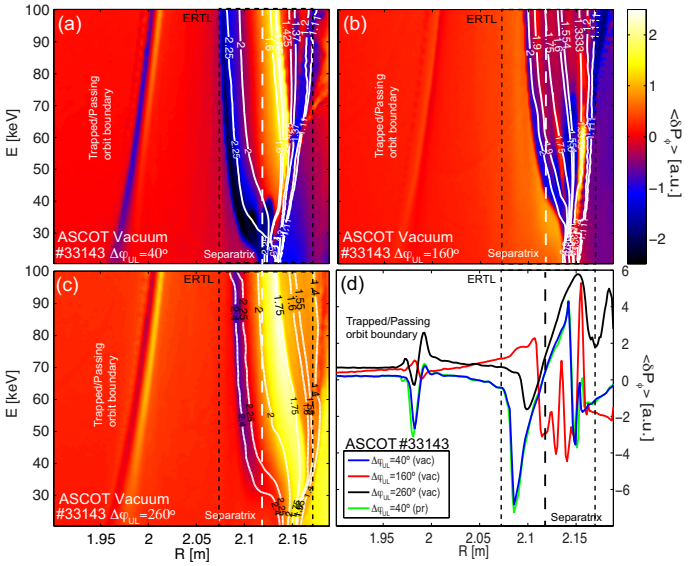

FIG. 3. AUG#33143. (a)-(c) $\langle \delta P_\phi \rangle$ as a function of particle energy and plasma major radius for a fixed pitch, $\Lambda = -0.5$, and (a) $\Delta\varphi_{UL} = 40°$, (b) $\Delta\varphi_{UL} = 160°$ and (c) $\Delta\varphi_{UL} = 260°$ together with contours of $\omega_b/\bar{\omega}_d$ ratio (white). (d) Radial profiles of $\langle \delta P_\phi \rangle$ for different $\Delta\varphi_{UL}$ configurations and energy E=50keV and pitch $\Lambda = -0.5$.

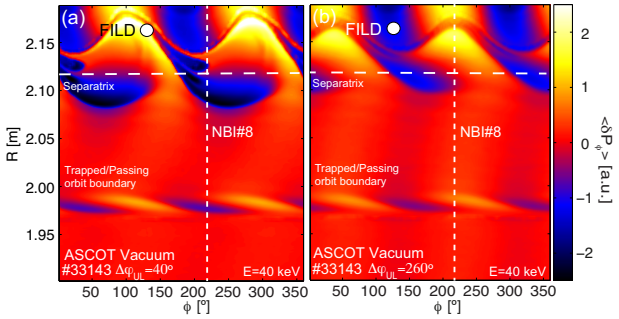

FIG. 4. AUG#33143. $\langle \delta P_\phi \rangle$ as a function of plasma major radius and toroidal angle for particles with E=60keV and pitch, $\Lambda = -0.5$ for: a) $\Delta\varphi_{UL} = 40°$ and b) $\Delta\varphi_{UL} = 260°$. White circles indicate de location of FILD detector.

the simulated losses using vacuum and MARS-F fields for $\Delta\varphi_{UL}$ between 0° and 150°. At $\Delta\varphi_{UL} = 40°$, the plasma response leads to a 20% enhancement of the fast-ion losses with respect to the vacuum approach, while at $\Delta\varphi_{UL} = 180°$ this difference is reduced to a 5%.

Edge Resonant Transport Layer - The energetic particle phase space affected by the externally applied 3D fields has been identified by computing the variation of the energetic particle toroidal canonical angular momentum, $P_\phi = mRv_\phi - ze\psi$, as a function of the perturbation poloidal spectrum. The variation in P_ϕ is related to radial transport, where a positive (negative) variation leads to an inward (outward) transport.

Figure 2(b) shows the energetic particle $\langle \delta P_\phi \rangle$ as a function of particle pitch-angle and plasma major radius for the main NBI injection energy, initial z on the midplane and a $\Delta\varphi_{UL} = 40°$. Clear structures are observed in both the trapped ($\Lambda \geq$ -0.5 at R=2.0m) and passing ($\Lambda \leq$ -0.5 at R=2.0m) regions, with the maximal variation located within 10 cm around the separatrix indicating that the transport is predominately resonant. Indeed non-structured (chaotic) $\langle \delta P_\phi \rangle$ regions are observed mainly for passing ions with R≥2.10m. The particle $\langle \delta P_\phi \rangle$ as a function of particle energy and perturbation poloidal spectrum for a given (NBI injection) pitch-angle, confirms that the transport is mainly resonant and located within 5 cm around the separatrix with a mild energy dependency and strong dependence of the perturbation poloidal spectrum. Figures 3(a)-(c) show the energetic particle $\langle \delta P_\phi \rangle$ as a function of particle energy and plasma major radius for the perturbation poloidal mode spectra that causes the maximum outwards (a) and inwards (c) transport. An intermediate transport value with clear structures around the separatrix is shown in Fig. 3(b). Figure 3(d), which is obtained from the results of figures 3(a)-(c), highlights in particular the transport of particles at 50 keV as a function of the plasma major radius. The most important transport is always located between R=2.08m and R=2.15m with the trapped-passing boundary highlighted for all perturbations at R≈ 1.98m. The impact of the plasma response on the particle radial transport for this plasma discharge is shown in green in Fig. 3(d) for $\Delta\varphi = 40°$ increasing the $\langle \delta P_\phi \rangle$ value by a maximum of 10%.

The patterns found in the $\langle \delta P_\phi \rangle$ for different $\Delta\varphi_{UL}$ can be understood by plotting the fast-ion geometrical resonances over the activated resonances calculated through $\langle \delta P_\phi \rangle$ as it is shown in Figs. 3(a)-(c). Geometrical orbital resonances were calculated in the E-R plane at the ratio $\omega_b/\bar{\omega}_d$ constant, where $\bar{\omega}_d$ is the average transit frequency and ω_b is the bounce frequency. In this context, a geometrical resonance will be considered linear if the frequency ratio can be expressed as $\omega_b/\bar{\omega}_d = n/p$ where n is the toroidal number, p is the bounce harmonic. Figures 3(a)-(c) show a clear matching between geometrical resonances and the maxima and minima of $\langle \delta P_\phi \rangle$. The dominant resonances are $\omega_b/\bar{\omega}_d = 2.25$ for $\Delta\varphi_{UL} = 40°$, $\omega_b/\bar{\omega}_d = 2$ for $\Delta\varphi_{UL} = 160°$ and $\omega_b/\bar{\omega}_d = 1.75$ for $\Delta\varphi_{UL} = 260°$. The matching between the maxima and minima of $\langle \delta P_\phi \rangle$ and the geometrical resonances indicates that, when the perturbation is applied, the ERTL is activated by a combination of linear and nonlinear resonances, but also the area corresponding to the trapped/passing boundary presents a significant $\langle \delta P_\phi \rangle$ due to a very high density of geometrical resonances at R=1.95-2.0m.

Most of the active resonances involved in the ERTL are nonlinear, which can be explained by considering a function describing a toroidally and poloidally varying field in the form $f(\mathbf{r}) = \sum_{n,m\in\mathbb{Z}} e^{in\xi - im\theta} f_{m,n}(r)$ [25], expressed

in terms of particle coordinates (r, θ, ξ). The projection of the perturbed magnetic field along the trajectory of an unperturbed trapped particle yields:

$$f(\mathbf{r}) = \sum_{n,m,p\in\mathbb{Z}} e^{i(n\bar{\omega}_d - p\omega_b - \omega_0)\tau} P_{n,m,p} \cdot f_{m,n}(\mathbf{r}) \qquad (1)$$

where τ is a time variable, $P_{n,m,p}$ is a projection operator along the unperturbed trajectory of the trapped particle. This expression provides the linear resonant condition given by $\frac{d}{d\tau}(\alpha\tau) = 0$ with $\alpha = n\bar{\omega}_d - p\omega_b$ for nearly stationary perturbations ($\omega_0 = 0$). We assume that the dominant effect of the magnetic perturbation is to produce a periodic modulation when the linear resonance condition is not satisfied. Considering that the modulation periodicity is given by the perturbation and all terms can be written as periodic functions, we have:

$$f(\mathbf{r}) \simeq \sum_{p,l\in\mathbb{Z}} e^{i(n\bar{\omega}_d - p\omega_b - \omega_0)\tau} e^{il(n\bar{\omega}_d - p_0\omega_b - \omega_0)\tau} P_{n,m,p} \cdot f_{m,n,l}(\bar{r}) \qquad (2)$$

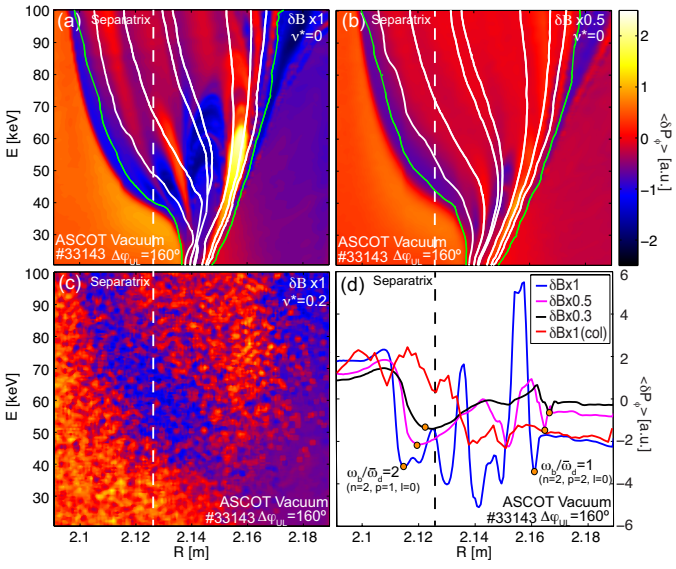

FIG. 5. AUG#33143. $\langle\delta P_\phi\rangle$ calculated for $\Delta\varphi_{UL} = 160°$ coil configuration using 3D field amplitude of: (a) $\delta B \times 1$ and (b) $\delta B \times 0.5$ and (c) $\delta B \times 1$ including collisions. Contours indicate linear (green) and nonlienar (white) resonances. (d) $\langle\delta P_\phi\rangle$ profiles for $\Delta\varphi_{UL} = 160°$ configuration at energy E=50keV using different δB amplitudes.

for a fixed value of n, m, where l is the nonlinear harmonic, $p = p_0 + p'$, p_0 is the primary bounce harmonic and p' is the additional bounce harmonic. From relation (2) the resonant condition is given by $(n\bar{\omega}_d - p\omega_b) + l(n\bar{\omega}_d - p_0\omega_b) = 0$, which can be written as:

$$\frac{\omega_b}{\bar{\omega}_d} = \frac{n(1+l)}{p_0(1+l) + p'} \qquad (3)$$

Using relation (3) we can now identify resonances triggered by a given value of $\Delta\varphi_{UL}$. By modifying the poloidal mode spectra of the perturbation, different resonances are activated with different amplitudes and radial transport direction (Figs. 3(a)-(d)). In the analysed shot, $n = 2$ is fixed due to the perturbation symmetry and p_0 and p' can take integer values reproducing most of the resonant structures in Figs. 3(a)-(c). In Fig. 3(d) it is shown that the effect of the applied $\Delta\varphi_{UL}$ on the amplitude of the resonant particle transport depends strongly on the ratio between the bounce and transit frequencies.

The role that the initial toroidal phase of the particles has with the perturbation is studied in Fig. 4(a) and (b) through $\langle\delta P_\phi\rangle$ for two different $\Delta\varphi_{UL}$. A clear $n = 2$ structure is observed on particle transport for both configurations along with a highlighting of the trapped passing boundary. Figure 4(a) shows how fast-ions generated by NBI#8 are injected in the least favourable toroidal location for $\Delta\varphi_{UL} = 40°$ configuration in terms of ion confinement, while $\Delta\varphi_{UL} = 260°$ presents the opposite situation (Fig. 4(b)).

To illustrate the impact of the perturbation amplitude on the intensity of the associated transport, a scan in amplitude is presented in Figs. 5(a) and 5(b). The observed effect of the perturbation amplitude on the behavior of $\langle\delta P_\phi\rangle$ is that, as we decrease the amplitude enough to pass a threshold, linear resonances ($l = 0$) still have a significant contribution while $\langle\delta P_\phi\rangle$ maxima associated with nonlinear resonances fade. Figure 5(d) shows radial profiles of $\langle\delta P_\phi\rangle$ for different perturbation amplitudes at a fixed energy to illustrate how linear resonances experience a gradual decrease for smaller amplitudes where nonlinear resonances sharply disappear.

To complete the analysis of the different sources that may have an impact on fast-ion transport, Coulomb collisions between energetic particles and the bulk plasma have been considered in realistic simulations using ASCOT (Fig. 5(c)). A widening of some of the resonant structures is observed with an overall reduced amplitude. Figure 5(d) shows calculations of $\langle\delta P_\phi\rangle$ with collisions included. The result is an overall reduction in peak $\langle\delta P_\phi\rangle$ changes as well as significantly less structures associated with individual resonances.

Conclusions - This letter shows that the fast-ion transport induced by externally applied 3D fields in a tokamak are caused by an Edge Resonant Transport Layer that depends on the fast-ion orbit topology, perturbation spatial spectrum and amplitude and plasma collisionality. The dominant resonant transport is mainly linear for small amplitude perturbations, but it becomes nonlinear as the amplitude increases to levels used routinely for RMP ELM suppression. When coulomb collisions are included, wave-particle resonance is less effective and, as a consequence, the particle transport decreases.

The tools utilized for this letter can not only be used to understand the experiment described here, but also to predict such experiments in future devices like ITER. Furthermore, this opens the possibility for future studies to optimize the operational scenarios based on the device needs, avoiding a critical degradation of fast-ion confinement.

This work has been carried out within the framework of the EUROfusion Consortium and has received funding from the Euratom research and training programme 2014-2018 under grant agreement No 633053. The views and opinions expressed herein do not necessarily reflect those of the European Commission.

[1] D. A. Spong, Phys. Plasmas **22**, 055602 (2015).
[2] T. C. Hender *et al.*, Nucl. Fusion **32**, 2091 (1992).
[3] T. E. Evans *et al.*, Nat. Physics **2**, 419 (2006).
[4] A. Loarte *et al.*, Nat Phys. **2**, 369 (2006).
[5] W. Suttrop *et al.*, Phys. Rev. Lett. **106**, 225004 (2011).
[6] S. A. Sabbagh *et al.*, Phys. Rev. Lett. **97**, 045004 (2006).
[7] A. Bortolon *et al.*, Phys. Rev. Lett. **110**, 265008 (2013).
[8] J.-K. Park *et al.*, Phys. Rev. Lett. **99**, 195003 (2007).
[9] C. Paz-Soldan *et al.*, Phys. Rev. Lett. **114**, 105001 (2015).
[10] M. Willensdorfer *et al.*, Phys. Rev. Lett. **119**, 085002 (2017).
[11] R. Nazikian *et al.*, Phys. Rev. Lett. **114**, 105002 (2015).
[12] Z. Unterberg *et al.*, Nucl. Fusion **50**, 034011 (2010).
[13] M. Garcia-Munoz *et al.*, Plasma Phys. Control. Fusion **55**, 124014 (2013).
[14] M. Van Zeeland *et al.*, Nucl. Fusion **55**, 73028 (2015).
[15] H. E. Mynick, Nucl. Fusion **26**, 491 (1986).
[16] J.-K. Park, Phys. Rev. Lett. **99**, 195003 (2007).
[17] K. Kim *et al.*, Phys. Rev. Lett. **110**, 185004 (2013).
[18] K. C. Shaing, Phys. of Plasmas **10**, 1444 (2003).
[19] K. C. Shaing *et al.*, Phys. of Plasmas **15**, 082506 (2008).
[20] T. Kurki-Suonio *et al.*, Plasma Phys. Control. Fusion **59**, 014013 (2017).
[21] W. Suttrop, A. Kirk, and others., Fusion Eng. Des. **84**, 290 (2009).
[22] M. Garcia-Munoz *et al.*, Rev. Sci. Instrum. **80**, 10 (2009).
[23] E. Hirvijoki *et al.*, Comput. Phys. Commun. **185**, 1310 (2014).
[24] Y. Liu *et al.*, Phys. of Plasma **7**, 3681 (2000).
[25] F. Zonca *et al.*, New J. Phys. **17**, 13052 (2015).